Journal of Building Engineering 86 (2024) 108626

Contents lists available at ScienceDirect

Journal of Building Engineering

journal homepage: www.elsevier.com/locate/jobe

Characterisation of new components of unequal-width welded I-beam–RHS-column connections

Javier Gracia *, Miguel Lozano, Carlos López-Colina, Miguel A. Serrano-López

University of Oviedo, Department of Construction and Manufacturing Engineering, Building DO7, Pedro Puig Adam St, 33204, Gijón, Spain

ARTICLE INFO

Keywords:
Steel connections
Experimental tests
Joint characterization
Component method
RHS

ABSTRACT

A study of two new components of welded I-beam–RHS-column connections with a beam-column width ratio lower than one is presented in this paper. In these connections, the usual failure mode is by yielding of the front faces (high indentation) due to the bending caused by tensile and compressive forces coming from the beam flanges. To this extent, twelve connections were tested to characterise the tube front face component (FFC) under tension and compression. Additionally, two connections with asymmetrical load were tested to characterise the tube lateral face component (LFC) under shearing. After the experimental campaign, finite element models were developed and calibrated to reproduce the experimental results accurately. Ultimately, the outcomes from the experiments and computational models provided sufficient information to suggest novel analytical equations for both components, thereby facilitating their analytical characterisation.

1. Introduction

Tubular sections are becoming increasingly popular as a choice for columns in the construction of steel buildings. The reason is that hollow sections have several advantages over traditional open profiles: structural efficiency and a more attractive appearance [1,2].

Open-section profiles, such as I-beam profiles, perform best when combining a beam with a tubular column (Rectangular Hollow Section RHS or Square Hollow Section SHS). This beam-column combination optimises the mechanical properties of both section types to the maximum: the tubular section to resist mainly the compression forces and the I-shaped section to resist bending.

The connections between these two types of sections can be welded or bolted. Bolted ones have been extensively studied [3–6]; they have the advantage that they can be manufactured in the workshop and, therefore, assembly on site is more straightforward. In contrast, welded joints have a more aesthetic appearance: no protruding angles, threads, or screws. In addition, they could transmit moments more easily. However, the main drawback is the welding process. Due to the heat generated, the base material can experience changes in its properties [7,8].

Both types of connections are mainly characterised by strength, stiffness, and rotation capacity. These properties are essential for a complete, precise, and optimal analysis of steel buildings. Without these properties, connections are designed only as pinned or rigid, even though most are semi-rigid.

The joint stiffness, resistance, and rotation capacity can be obtained through experiments, numerical models [9] or analytical formulation. Among these methods, the component method is the most widespread analytical method to characterise a joint. In this methodology, implemented by Eurocode 3 [10], the joint is subdivided into different components represented by translational and

* Corresponding author.
E-mail address: graciajavier@uniovi.es (J. Gracia).

https://doi.org/10.1016/j.jobe.2024.108626
Received 24 May 2023; Received in revised form 3 January 2024; Accepted 23 January 2024
Available online 6 February 2024

rotational springs with a given stiffness. These individual springs are assembled into a single rotational spring to simulate the behaviour of the complete joint in a global analysis of the structure.

The main issue with the component method is that it requires precise analytical equations for each component, both for strength and stiffness. In the case of components for columns based on open profiles (IPE or HEB), the equations are included in Eurocode 3 [10]; on the contrary, in the case of tubular column connections, the most critical design guidelines on hollow sections [2] and column connections [11] indicate that the prediction of the stiffness of the beam to RHS tubular column connections is still not possible with an analytical method because some components of the tubular column have not been characterised yet.

Furthermore, limited experimental and FEM moment-rotation curves can be found, such as those by Lu [12]. However, more recent research articles have tried to fill gaps in knowledge of component behaviour for hollow section connections [13–17]. Nevertheless, the most significant review work on this subject has been conducted by Jaspart and Weynand [18,19]. Their work provides an exhaustive review of the equations found in academic literature for applying the component method to joints involving steel hollow sections. Despite this, their work highlights the persisting knowledge deficit regarding welded I-beam-to-RHS-column connections, particularly about the stiffness of the individual components and the methodology for assembling them to achieve the rotational stiffness of the complete joint.

Concerning I-beam to RHS column connections, when the β (beam width/column width) ratios are equal to one and the load is symmetrical, the behaviour of the connection can be easily simplified through three components: the column web under shear, the column lateral face under compression and tension. In Ref. [20], the authors of this paper presented analytical expressions for the lateral faces under tension or compression, which are the main active components when $\beta = 1$. However, to fully characterise this type of joint, it is necessary to analyse the front face component, which is the main one active when $\beta < 1$, and the lateral face component when the load is asymmetric, i.e., lateral faces under shear.

In the case of $\beta < 1$, it has been verified that the usual failure mode is by yielding of the front faces (high indentation) due to the bending caused by tensile and compressive forces coming from the beam flanges. Moreover, when an asymmetric bending moment is applied at the joint, shearing deformation occurs at the lateral faces of the tube column (web panels). These conclusions have been recently confirmed by Teixeira et al. [21]. They presented an experimental and numerical study to obtain the stiffness of welded I-beam to RHS column connections with values of $\boldsymbol{\beta}$ equal to 0.4, 0.5 and 0.6.

Therefore, to complete our previous research [20], this paper will focus on the characterisation, including both stiffness and resistance, of the following components:

- Front face component (FFC) under tension and compression for a beam-column joint with a width ratio $\beta < 1$.
- Lateral face component (LFC) under shearing.

With this primary aim, twelve connections with symmetrical loads with a width ratio of less than one and two more connections with asymmetrical loads but equal width ratios were tested. These tests, including those published in Ref. [22], were utilised for calibrating a numerical model based on finite elements. From the analysis of the curves obtained by both procedures, analytical equations are proposed for the stiffness and resistance of each component. Finally, two different analytical models will be applied to obtain the moment-rotation curve of joints with a value of $\beta < 1,$ allowing their characterisation.

2. Experimental program

The experimental programme was planned in five distinct phases, throughout which 47 full-scale specimens underwent rigorous testing. Phase 1 comprised eight trials, Phase 2 similarly consisted of eight, Phase 3 incorporated fourteen, Phase 4 included fifteen and, ultimately, Phase 5 contained a mere two. The disparities between one phase and another can be attributed to the measurement apparatus, the testing machinery, the beam-column combinations, the specific type of welding under consideration, or the symmetry of the load applied to the joint.

The experimental programme in this study corresponds to a portion of the specimens from phases 1, 2, and 3 and all the specimens

Table 1
Summary of the section combinations and width ratio.

Specimen	Column RHS profile	Beam IPE profile	$\boldsymbol{\beta}$
1.6	100 × 100 × 6	140	0.7
1.8	150 × 100 × 4	140	0.7
2.6	200 × 100 × 6	140	0.7
2.8	200 × 100 × 4	140	0.7
3.2	150 × 150 × 6	240	0.8
3.3	150 × 150 × 6	180	0.6
3.6	200 × 150 × 6	240	0.8
3.7	200 × 150 × 6	180	0.6
3.10	250 × 150 × 6	240	0.8
3.11	250 × 150 × 6	180	0.6
3.13	250 × 150 × 8	240	0.8
3.14	250 × 150 × 8	180	0.6
5.1	200 × 150 × 6	300	1.0
5.2	200 × 150 × 8	300	1.0

from phase 5. The remaining specimens were presented in Ref. [20] to characterise the lateral face component of the RHS column, both in tension and compression, when the width ratio was equivalent to 1.0. Conversely, the results of phase 4, which concentrated on studying the joint behaviour when the beam web is welded, were presented in Ref. [22].

Hence, the specimens from phases 1, 2 and 3 presented in this paper correspond to specimens with a width ratio of less than 1.0. These samples were utilised to characterise the front face component of the RHS column in both tension and compression. Lastly, the results of Phase 5, with asymmetric loading and equal width ratio, were employed to characterise the lateral face component of the RHS column under shear loads.

The upcoming section will illustrate the joint configurations and the results of this experimental campaign for welded I-beam-to-RHS-column connections.

2.1. Specimens and test setup

Table 1 shows the section combinations for column and beam and the width ratio of the 14 tested connections. The first number of the specimen name refers to the experimental phase. The beam was attached to the shortest side of the RHS in all specimens.

2.1.1. Experimental phase 1

The first two specimens in Table 1 belong to this phase. The objective of these tests was to obtain the resistance of the joint.

Phase 1 tests were conducted utilising an MTS universal testing machine with a load capacity of 1 MN, and the load was applied with displacement control at a 4 mm/min rate. The test configuration is shown in Fig. 1. The general dimensions are identical for all specimens in Table 1 except for specimen 2.8. For this specimen, the column length is 990 mm instead of the standard 900 mm.

2.1.2. Experimental phases 2 and 3

This phase comprises ten specimens (ranging from 2.6 to 3.14), as outlined in Table 1. The moment-rotation curves were obtained for each test as in the previous phase. From this information, the experimental initial strength and stiffness were identified.

On this occasion, a digital image correlation system, ARAMIS 5 M, measured displacements, rotations, and deformations. As per the guidelines provided by the manufacturer, utilising two lenses with a focal length of 23 mm is suggested to capture the specific area of interest.

Two distinct segments (100 mm) were utilised to evaluate the joint rotation: a vertical segment and a horizontal segment, as depicted in Fig. 2. Furthermore, the column bending and rotation are null due to the joint symmetry. However, the rotation of the column was also monitored to verify its vertical alignment. The rotations obtained with both segments demonstrated a less than 0.2 % variation. Therefore, it was unnecessary to discount either the effect of the beam bending or that of the column.

Finally, the specimens were tested on a reaction frame comprising HEB 300 sections. The actuator used is an IBERTEST model with a 500 kN hydraulic actuator. As shown in Fig. 3, the actuator was attached to the lower flange of the upper beam of the reaction frame.

2.1.3. Experimental phase 5

The last two specimens in Table 1 correspond to this phase. The objective of this phase was to investigate the behaviour of the lateral faces of the RHS column under shearing load. For this reason, only one beam was welded to the column. The beam was chosen with the same width as the column to avoid any influence of the front face component. The actuator was placed at the end of the beam. With one side load, this setup (Fig. 4) guaranteed shearing forces at the lateral faces of the RHS column.

The specimens were tested on the same reaction frame and with the same actuator as phases 2 and 3. Rotations, displacements, and

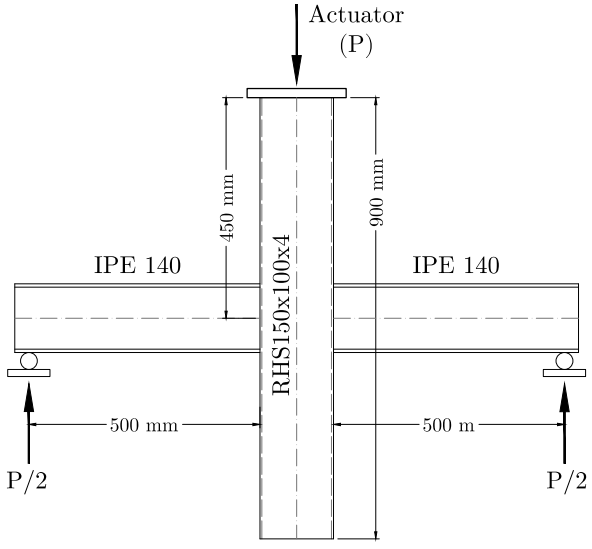

Fig. 1. Loading setup for specimens of phases 1, 2 and 3. Dimensions and the specific test corresponded to specimen 1.8 (RHS 150 × 100 × 4 and IPE 140).

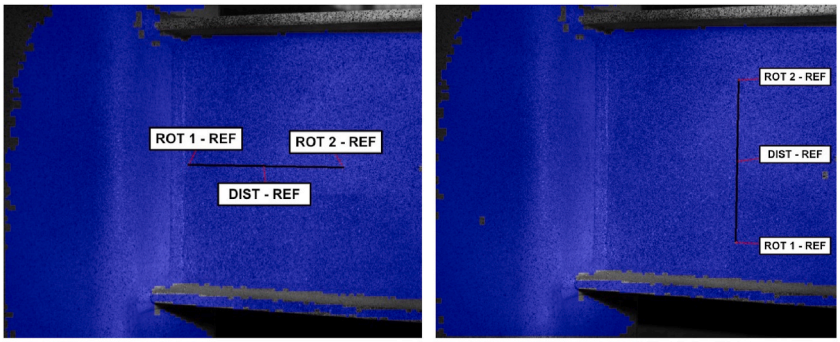

Fig. 2. Measurement marks at the centre of the beam web (a) and at 100 mm from the tube (b).

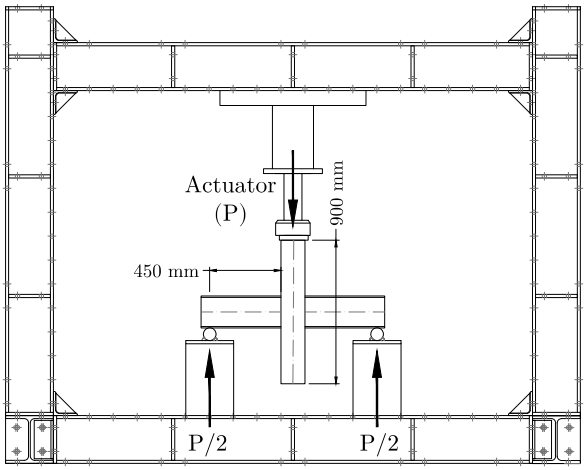

Fig. 3. Experimental setup with the reaction frame for tests on phases 2 and 3.

deformations were also measured using the same digital image correlation system as before, with the only difference being the use of lenses with a focal length of 12 mm to visualise the entire specimen.

The joint rotation was calculated by subtracting the column from the beam rotation. As mentioned in the previous section, the

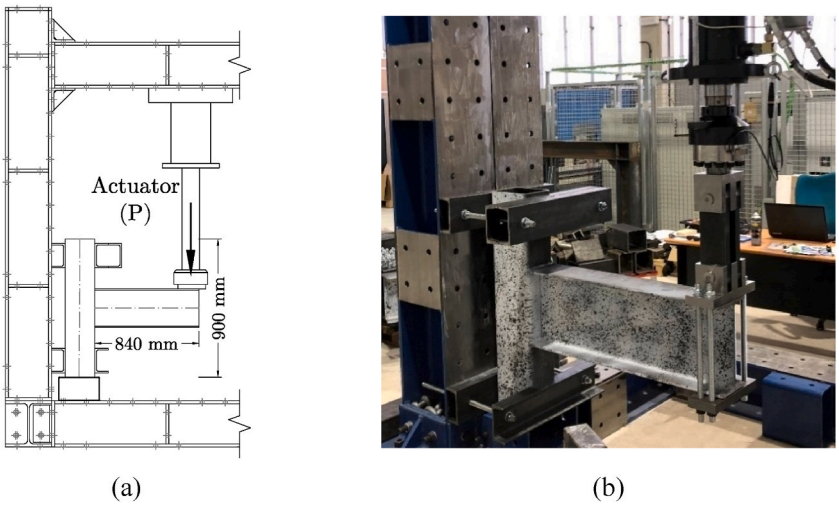

Fig. 4. Experimental setup of phase 5.

rotation measurements were conducted using vertical and horizontal segments. Like the earlier phases, the rotations were virtually identical. Therefore, it was unnecessary to discount any additional rotation due to the bending of the parts.

2.2. Experimental results

A summary of the main results obtained from the experimental campaign is presented below. The results are shown in two parts. The first part covers results corresponding to the study of the frontal face component with $\beta < 1$ (experimental phases 1, 2 and 3). The second part covers the results of experimental phase 5 with $\beta = 1.0$, corresponding to the study of the lateral face component of the column working under tension, compression, and shearing.

2.2.1. Results of phases 1, 2 and 3

Table 2 shows the moment resistance (M_R), ultimate rotation (Φ_R) and the initial rotational stiffness ($S_{j,exp}$) of the tested joints for the specimens of phases 1, 2 and 3. The initial rotational stiffness was calculated only for phases 2 and 3 specimens. The values were estimated as the mean slope of the curve measured from the origin to a rotation corresponding to an indentation in the frontal face of the column of 0.33 % of b_o (column width). This value is 1/3 of the 1% b_o indentation limit, corresponding to the literature serviceability limit state [2].

Regarding the apparent effect of the width ratio on the stiffness, Fig. 5 shows an illustrative surface regression of the experimental values of rotational stiffness ($S_{j,exp}$), normalised by dividing it by the beam stiffness (EI_b/L_b). A reference value of 20 times the beam depth was used for the beam length L_b. The approximate response surface shows that the two selected variables, column thickness t_0 and width ratio β, have a clear influence on the relative stiffness of the joint, the last being the most important.

It is worth noting that, regarding the relative stiffness, the values of 0.5, 8 and 25 are the values stated in EC3 for the limits for nominally pinned joints, rigid joints in non-sway frames and rigid joints in all frames, respectively. Therefore, this shows that typical joints are at least semi-rigid and can easily reach the nominally rigid boundary by increasing the width ratio β. The values of the mentioned relative stiffness and the corresponding stiffness classification according to Eurocode are also presented in Table 2.

The characterisation of the failure load, M_R, was estimated by two different procedures, with the value rendered in the table the first criterion reached:

- When the maximum value of the moment-rotation curve is reached (specimens marked with an asterisk in Table 2).
- When the IPE flange indentation into the tube (frontal face) was greater than 3% of b_o [23] (specimens without an asterisk in Table 2).

Figs. 6–8 show the moment rotation curves for specimens with IPE 140 beam, IPE 180 beam and IPE 240 beam, respectively. Each plot shows a vertical dotted line, indicating the value where the rotation equals an indentation of 3 % of b_o [23].

All specimens show nonlinear behaviour from an early stage of the experiment and large rotation capacities. However, an initial stiffness can be identified before the indentation of the flanges of the beam into the frontal face of the tube is evident. After this point, a softening of the stiffness is prominent due to the yielding of the frontal face of the column near the contact zone of the beam flanges with the column.

For the same column and beam, specimens with a thicker wall tube presented a higher M_R: specimen 2.6 vs 2.8, specimen 3.14 vs 3.11 and specimen 3.13 vs 3.10. In joints where solely h_0 is altered (specimen 3.2 compared to 3.6 and specimen 3.3 compared to 3.7), the increase in M_R is moderate, approximately 15 % greater for columns featuring reduced depth.

The slight difference in stiffness observed between specimen 3.3 vs 3.7 (Fig. 7) and specimen 3.2 vs specimen 3.6 (Fig. 8) can be attributed to the stiffness of the lateral face component described in Ref. [20]. Equation (5) illustrates that the connection stiffness relies on various components, notably the stiffness of the lateral face (k_{LF}) and the stiffness of the frontal face (k_{FF}). According to Ref. [20], the value of k_{LF} is inversely proportional to the width of the lateral face, b_0. This explains why the stiffness of specimens 3.6 and 3.7 is lower compared to that of specimens 3.2 and 3.3.

Regarding the failure mode, Fig. 9 shows specimen 2.8 after testing. As expected, when the width ratio is lower than one, a substantial indentation becomes apparent within the contact zone between the tube and the compressed flange of the IPE. On the

Table 2
Experimental results of moment resistance, rotation, initial rotational stiffness for specimens from phases 1, 2 and 3, and stiffness classification.

Specimen	M_R [kNm]	Φ_R [rad]	$S_{j,exp}$ [kNm/rad]	$\frac{S_{j,exp}}{EI_b/L_b}$	Stiffness class
1.6*	18.52	0.038	–		
1.8	7.51	0.044	–		
2.6	17.56	0.045	2582.0	6.36	Semi-rigid
2.8	9.55	0.045	1212.5	2.99	Semi-rigid
3.2	43.10	0.039	6464.2	27.30	Rigid (all)
3.3	19.64	0.053	1446.1	4.58	Semi-rigid
3.6	37.86	0.040	6074.8	25.66	Rigid (all)
3.7	16.77	0.053	1258.9	3.99	Semi-rigid
3.10	46.77	0.039	5894.1	24.89	Rigid (all)
3.11	22.70	0.053	1901.8	6.02	Semi-rigid
3.13	69.41	0.040	8649.5	36.53	Rigid (all)
3.14	33.27	0.053	2418.0	7.66	Semi-rigid

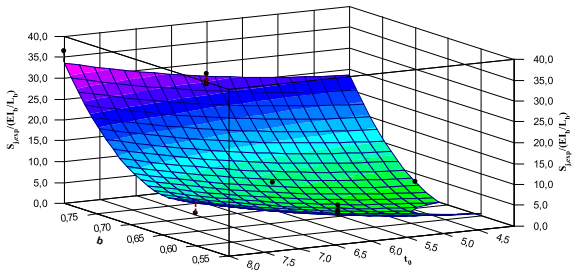

Fig. 5. Illustrative surface response for the relative stiffness.

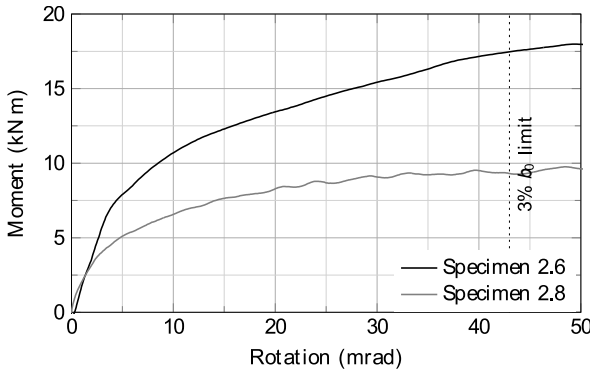

Fig. 6. Moment rotation curves for specimens with IPE 140 beam ($\beta = 0.7$).

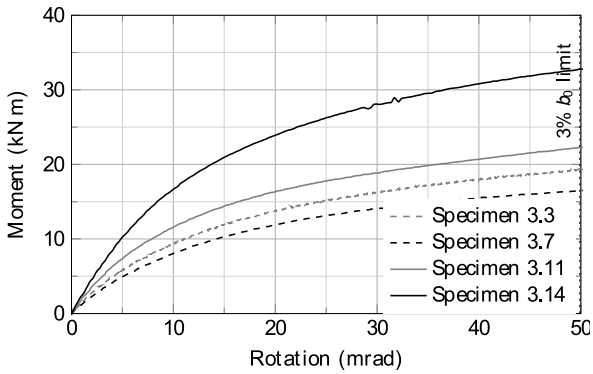

Fig. 7. Moment rotation curves for specimens with IPE 180 beam ($\beta = 0.6$).

contrary, tearing appeared when the deformation was prominent in the tension zone.

2.2.2. Results of phase 5

Fig. 10 displays the tube sidewall strain contour map under unilateral loading. As shown in the figure, the bending moment transmitted by the beam can be decoupled in two forces, each located at the centroid of the beam flanges. These forces induce a complex state of strains and stress at the lateral sides of the column: tensile stress at the upper beam flange (depicted in blue), compressive stress at the lower beam flange (depicted in red), and shear stress between the upper and lower beam flanges (corresponding to the area between the blue and red regions).

Moment rotation curves obtained for both specimens, 5.1 and 5.2, are shown in Fig. 11. As expected, the ultimate moment and initial stiffness are more significant for specimen 5.2. The only difference between both specimens is the thickness of the wall tube. The thickness of specimen 5.2 (8 mm) is 33% larger than that of specimen 5.1 (6 mm).

Finally, Table 3 shows both specimens' moment resistance, M_R, and initial rotational stiffness, $S_{j,exp}$. The ultimate moment of specimen 5.2 is 30 % larger, and the initial stiffness is 36 % higher.

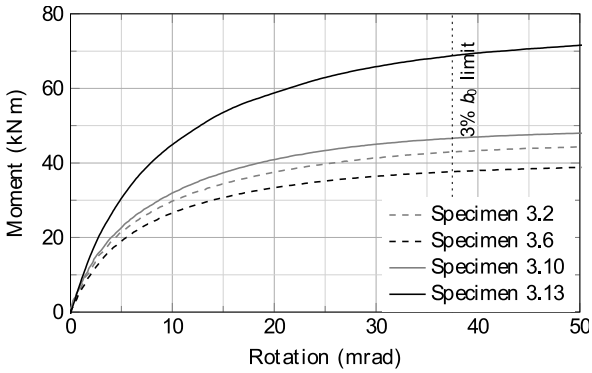

Fig. 8. Moment rotation curves for specimens with IPE 240 beam ($\beta = 0.8$).

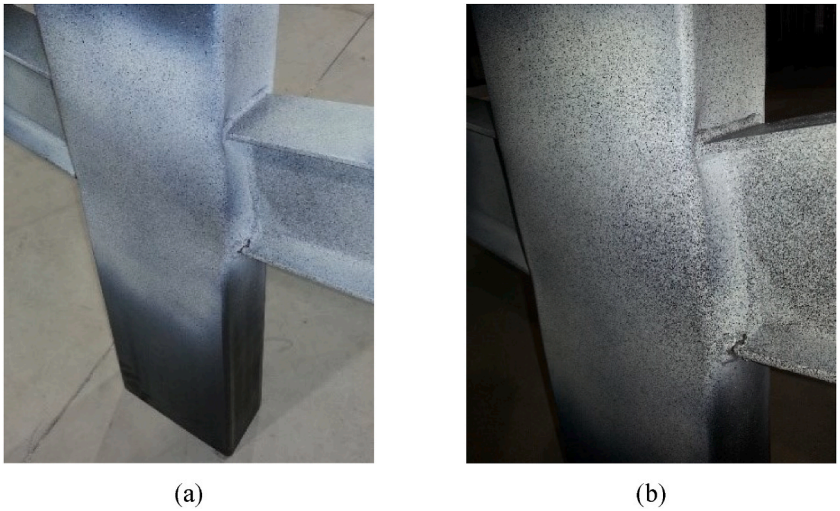

Fig. 9. Indentation in specimen 2.8.

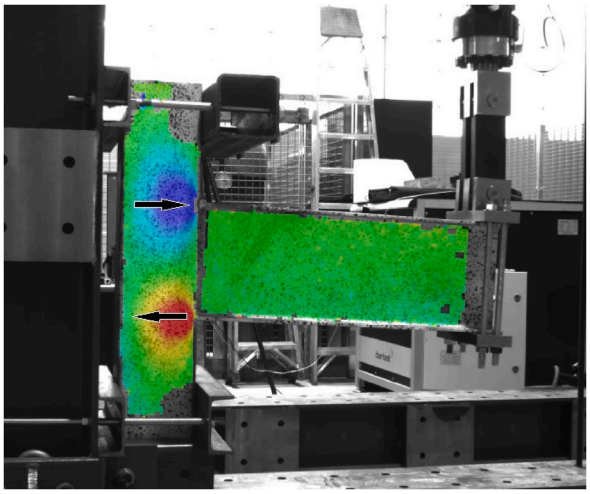

Fig. 10. Strains from digital image correlation system for specimen 5.2.

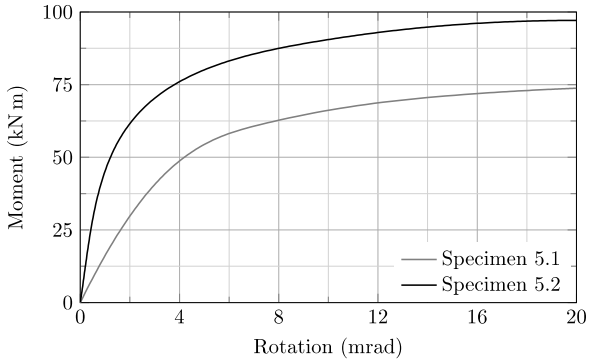

Fig. 11. Moment rotation curve for phase 5 specimens.

Table 3
Experimental moment resistance and initial rotational stiffness for phase 5 specimens.

Specimen	M_R [kNm]	$S_{j,exp}$ [kNm/rad]
5.1	74.70	16 415
5.2	97.30	22 411

3. Finite element model

Hereafter, the description and results of the computational work are presented. The welded I-beam–RHS-column connection experiments were reproduced using ANSYS 17.0 finite element software [24]. Due to the large number of simulations, a parametrical model was developed that allows loading different specimen geometries by changing key parameters such as dimensions and material properties. In total, 14 simulations were performed replicating the 14 specimens of the experimental campaign.

3.1. Description of the finite element model

The members and welds were modelled with element Shell 181 of the ANSYS library. This element consists of four nodes, each with six degrees of freedom, making it appropriate for simulating significant rotations and deformations. Furthermore, it is the best choice for modelling non-linearities [22].

Only one-half of the joint was modelled to speed up computation by applying a symmetry constraint. The elements that modelled the weld beads had thickness equal to the weld throat, and the entire model was developed by considering elements on the mid-surface of the plates (flanges and web in the beam and the tube walls).

This type of modelling was previously validated, calibrated, and tested by the authors against some experimental tests on I-beam joints with RHS columns published by the University of Delft [12]. Additional FEMs with brick and tetrahedral elements were also tested, but no significant differences in the results were found, so the increase in complexity and computational time was not justified [25].

The material model adopted in the analysis was elastic-plastic with bilinear isotropic hardening. The slope of the plastic portion was determined by dividing Young's Modulus by 100, as per the recommendation in EC3-1-5 [26]. This slope begins at the yield limit, f_y, which was assumed to be uniform throughout the section by taking the average yield limit based on EC3-1-3 [27] and considering the material properties of the faces as input, as suggested by the authors in Ref. [28]. This transformation is described by Eq. (1).

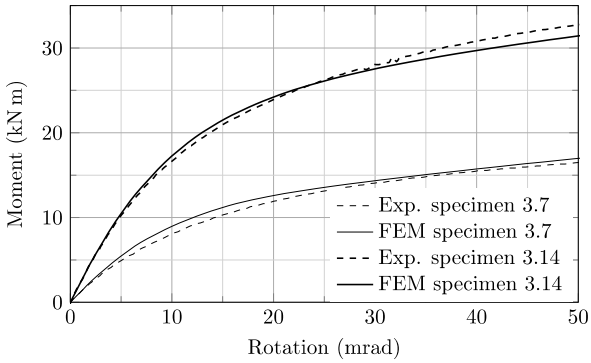

Fig. 12. Comparison of moment-rotation curves (test vs FEM) for specimens with $\beta = 0,6$.

$$f_y = f_{yo} + 28\frac{t_0^2}{A_0}\left(f_{uo} - f_{yo}\right) \quad (1)$$

Where f_{u0} and f_{y0} are the ultimate stress and yield limit of the face of the RHS (obtained from tensile coupon tests), respectively, A_0 is the area of the cross-section, and t_0 is the wall tube thickness.

3.2. Validation of the finite element model

The moment-rotation curve for all experimental tests was simulated and processed using finite element models under identical conditions to those in the experimental campaign. Then, computational curves were analysed to identify rotational stiffness ($S_{j,FEM}$) and the moment resistance ($M_{R,FEM}$).

Comparisons of experimental and simulated moment-rotation curves are presented below. They are arranged so that each pair of curves corresponds to the same value of β. Thus, Fig. 12 shows joints between IPE180 and tubes with 150 mm front face ($\beta = 0{,}6$), and Fig. 13 shows joints between IPE240 and tubes with 150 mm front face ($\beta = 0{,}8$). For all the values of $\boldsymbol{\beta}$ tested, the numerical model effectively captures the overall behaviour of the joint.

Table 4 summarises the moment resistance ($M_{R,FEM}$) and the initial rotational stiffness ($S_{j,FEM}$) obtained from the FE model, along with the error between experiments and FEM models for both initial stiffness ($D_{if,S}$) and moment resistance ($D_{if,MR}$). As described in Section 2.2.1, the resistances were defined in Table 2 by the criterion that was reached first, i.e., the maximum value from the moment-rotation curve or the moment when the deformation of the front face of the tube reaches 3 % of b_0 [23].

Finally, Figs. 14 and 15 show a graphical comparison between experimental and simulated values of stiffness and resistance, respectively. In both figures, the diagonal of the graph signifies the location where the experimental and simulated values coincide, whilst the dashed lines depict the locus of points with an error of ±10 %. In the case of stiffness, the average value of the deviation is 13,8 %, while the average value of the deviation for the moment resistance is 8,4 %. As shown in the figures, the results show a significant alignment between experimental and FEM models when assessing both the initial rotational stiffness and resistance.

4. Analytical proposal for new componentS

After conducting experimental tests and simulations, it was confirmed that the width ratio β is one of the determining factors in the failure mode of the connections. For $\beta = 1$, the failure modes and components were presented in Ref. [20].

For $\beta < 1$, the usual failure mode was by yielding of the front faces due to the bending produced by the tensile and compressive stresses transmitted by the beam flanges. In the compressive zone, there was more significant deformation in the front than in the lateral face, resulting in high indentation. On the other hand, in the tensile zone, the front face of the tube also deformed considerably before reaching a brittle fracture of the weld.

In double-sided connections featuring symmetrical bending moments, the shearing load impact on the lateral face of the rectangular hollow column is null. Nonetheless, characterising this component becomes imperative for connections involving a single-sided beam or asymmetric moments.

4.1. Characterisation of the stiffness of the front face component (FFC)

For connections with a $\boldsymbol{\beta}$ factor less than one, the experimental results demonstrated an apparent reduction in stiffness and resistance compared to connections with $\beta = 1$. This reduction is due to the additional deformation in the front face of the joint that is added to that produced on lateral faces. Therefore, to characterise the stiffness and strength of this type of joint, it is necessary to obtain the stiffness coefficient of the front face under compression, $k_{FF,C}$, and under tension, $k_{FF,T}$. These new components will be assembled with the components studied in Ref. [20] (lateral face under compression, $k_{LF,C}$, and under tension $k_{LF,T}$) into a single rotational spring to simulates to simulate the behaviour of the complete joint in a global analysis of the structure.

The experiments indicated that the deformation observed on the front face of the tube remained consistent, regardless of whether the force originated from the compressed or tensile flange, with only the force direction altering. As a result, the stiffness coefficient of

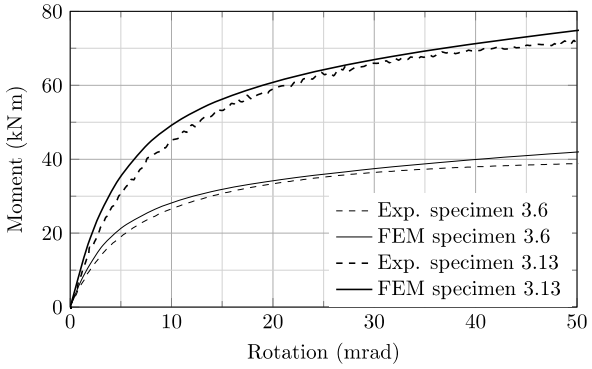

Fig. 13. Comparison of moment-rotation curves (test vs FEM) for specimens with $\beta = 0{,}8$.

Table 4
Numerical results of resistance and initial stiffness for specimens of phases 1, 2 and 3.

Specimen	$M_{R,FEM}$ [kNm]	$\Phi_{R,FEM}$ [rad]	$S_{j,FEM}$ [kNm/rad]	$D_{if,MR}$ [%]	$D_{if,S}$ [%]
1.6	20.06	0.038	–	8.3%	–
1.8	9.57	0.044	–	27.4%	–
2.6	18.47	0.045	2368.29	5.2%	−8.3%
2.8	10.13	0.045	1310.44	6.1%	8.1%
3.2	45.49	0.039	7306.80	5.5%	13.0%
3.3	19.00	0.053	1210.94	−3.3%	−16.3%
3.6	39.83	0.040	6867.97	5.2%	13.1%
3.7	17.30	0.053	1210.68	3.2%	−3.8%
3.10	50.04	0.039	7576.23	7.0%	28.5%
3.11	20.26	0.053	1370.42	−10.7%	−27.9%
3.13	71.22	0.040	9995.20	2.6%	15.6%
3.14	31.94	0.053	2324.62	−4.0%	−3.9%

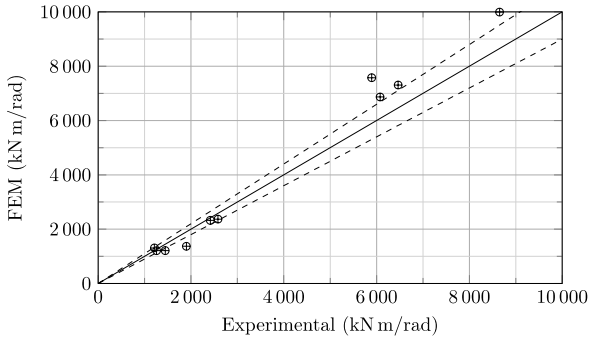

Fig. 14. Comparison of rotational initial stiffness S_j (Experimental vs FEM).

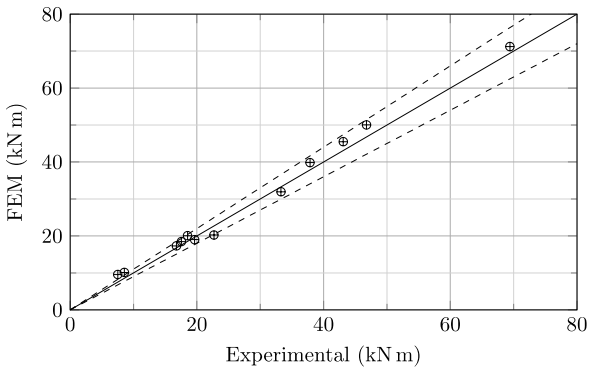

Fig. 15. Comparison of moment resistance M_R (Experimental vs FEM).

the compressed component $k_{FF,C}$ is like that of the tensile component $k_{FF,T}$.

Three different proposals for calculating the analytical stiffness of the component were adapted to these joints and then assessed. The first proposal, based on the expression developed by de Thai and Uy [6] for joints with blind bolts, did not yield satisfactory results. The second proposal was a modification of the expression proposed by Elghazouli [3] for connections between universal (UB) and RHS columns with angle profiles and blind bolts. The original expression was:

$$k_{FF,1} = \frac{\pi \bullet t_0}{12 \bullet (1-\nu^2) \bullet C_t \bullet \left(\frac{b_0}{2}\right)^2} \tag{1}$$

Where t_0 is the thickness of the hollow section, ν is the modulus of Poisson, b_0 is the width of the hollow section, and C_t was originally a constant coefficient equal to 0.18 calibrated from a finite element model. For the connections studied in this paper, C_t was adapted to consider the value of β, which affects the stiffness of the component, resulting in the modified expression:

$$C_t = -0.08 \bullet \beta + 0.07 \tag{2}$$

The third proposal was based on the model by Grotmann and Sedlacek [29]. The original expression was:

$$k_{FF,2} = \frac{4 \bullet L_{eff} \bullet t_0^3}{b_0^3 \bullet (1-\beta^2) \bullet (0.6 - 0.1 \bullet \beta)} \tag{3}$$

Here, b_0 is the width of the hollow section, and L_{eff} is the effective length. L_{eff} was adapted to consider the welds and the value of β for the connections studied in this paper, resulting in the modified expression:

$$L_{eff} = t_f + 2 \bullet \sqrt{2} \bullet a + 2 \bullet b_0 \bullet \sqrt{1-\beta} \tag{4}$$

Finally, to compare the stiffness of the joint obtained from the proposed expressions with the experimental values, the stiffness of each joint has been evaluated. The mechanical model of the joint used to assemble the stiffness of each component is shown in Fig. 16. Under this configuration, and adopting the equation proposed by Eurocode 3 [10] (equation 6.27), the final expression to obtain the numerical stiffness of the joint is as follows:

$$S_j = \frac{E \cdot z^2}{\frac{1}{k_{LF,C}} + \frac{1}{k_{FF,C}} + \frac{1}{k_{LF,T}} + \frac{1}{k_{FF,T}}} = \frac{E \cdot z^2}{\frac{2}{k_{LF}} + \frac{2}{k_{FF}}} \tag{5}$$

Table 5 shows the component stiffness and the joint rotational stiffness calculated with the last two proposals, $k_{FF,1}$ and $k_{FF,2}$. Specimens marked with an asterisk correspond to experiments presented in Ref. [22], which are included here to complete the analytical study.

Finally, Figs. 17 and 18 show a graphical comparison of the stiffness obtained experimentally and numerically (FEM model) against values obtained with both proposed models, $k_{FF,1}$ and $k_{FF,2}$. In both figures, the diagonal of the graph signifies the location where the experimental and simulated values coincide, and the dashed lines represent the locus of the points with an error between ±10 %.

Except for the result of specimen 2.3, the comparisons with the analytical model $S_{j,k_{FF1}}$ show an acceptable fit (refer to Fig. 17). The average error concerning both the experiments and the finite element model is 15%. Furthermore, the analytical approach is generally conservative. Lastly, the comparisons with the analytical model $S_{j,k_{FF2}}$ exhibit better results (see Fig. 18), with an average error of 11% with respect to the experimental tests and 15% with respect to the finite element models.

4.2. Characterisation of the resistance of the front face component (FFC)

Failure due to strength on the front face can occur through two different procedures: bending failure and shear failure. In both cases, failure can occur in the compression zone as well as in the tension zone. In addition, it is also necessary to consider failure due to the effective width of the flange.

A total of two analytical proposals were studied. For either of the two, the resistance moment is obtained from the following expression:

$$M_R = \min(F_R) \bullet z \tag{6}$$

where F_R is the value of the component resistance for any of the considered failures.

The first analytical proposal was based on CIDECT Project 16F by Weynand et al. [18]. The proposed expression to characterise the resistance to bending was:

$$F_R = (0.5 \bullet l_{eff,1,a} + l_{eff,2,a}) \bullet m_{pl} \tag{7}$$

Where l_{eff} is the normalised effective length and m_{pl} is the plastic moment of the beam. In the case of this type of joint, the proposed expression for the value of $(0.5 \bullet l_{eff,1,a} + l_{eff,2,a})$ was:

$$\begin{cases} 2 \bullet \dfrac{2 + 2.8 \bullet \beta}{\sqrt{1 - 0.9 \bullet \beta}}, \; if \; \eta > 2 \bullet \sqrt{1-\beta} \\ \dfrac{2 + 2.8 \bullet \beta}{\sqrt{1 - 0.9 \bullet \beta}} \bullet \left(1 + \dfrac{\eta - \frac{t_f}{b_0}}{2 \bullet \sqrt{1-\beta} - \frac{t_f}{b_0}} \right), \; if \; \dfrac{t_f}{b_0} \le \eta < 2 \bullet \sqrt{1-\beta} \end{cases} \tag{7}$$

where $\eta = \frac{h_b}{b_0}$.

In the case of resistance to shear punching, the expression used was the one proposed in section (d) of Annex C of the CIDECT 16F report [18]:

$$F_{R,p} = \frac{b_{eff} \cdot f_{y0} \cdot t_0}{\sqrt{3}} \tag{8}$$

Where b_{eff} is the effective width, calculated according to:

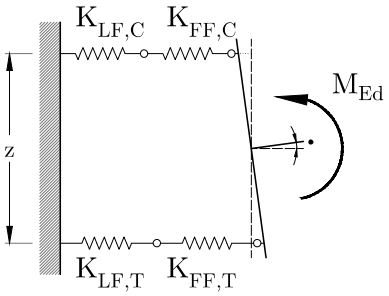

Fig. 16. Mechanical model of the joint for $\beta < 1$.

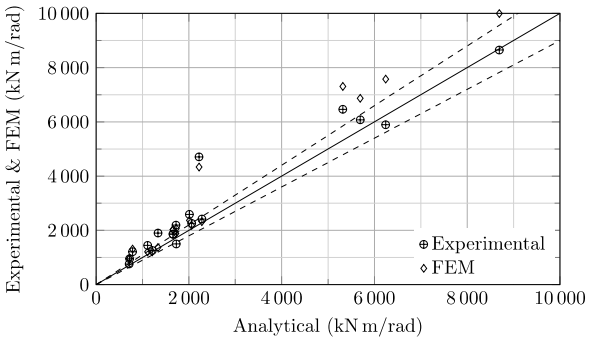

Fig. 17. Comparison of analytical initial stiffness $S_{j,k_{FF1}}$ vs experimental and FEM values.

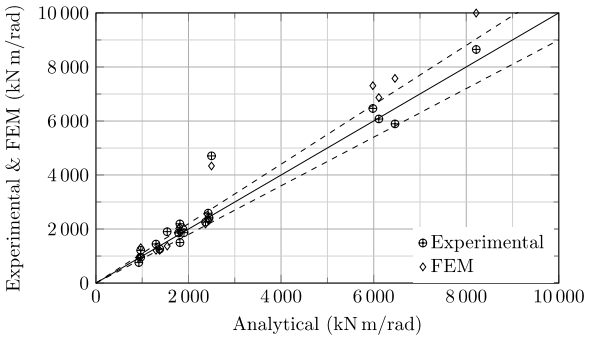

Fig. 18. Comparison of analytical initial stiffness $S_{j,k_{FF2}}$ vs experimental and FEM values.

$$b_{eff} = \begin{cases} t_f + b_{eff,p} \; if \; \eta > 2 \bullet \sqrt{1-\beta} \\ \dfrac{t_f + b_{eff,p}}{2} \bullet \left(1 + \dfrac{\eta - \dfrac{t_f}{b_0}}{2 \bullet \sqrt{1-\beta} - \dfrac{t_f}{b_0}} \right), if \; \dfrac{t_f}{b_0} \leq \eta < 2 \bullet \sqrt{1-\beta} \end{cases} \tag{9}$$

and $b_{eff,p}$ is the punching effective width, calculated as:

$$b_{eff,p} = \frac{10}{\frac{b_0}{t_0}} \bullet b_f \leq b_f \tag{10}$$

The second analytical proposal (FFR1) is based on the expression proposed by Grotmann and Sedlaceck [29]. In this case, the equation for the resistance force (F_R) is as follows:

$$F_R = \frac{2 \bullet t_0^2 \bullet f_{yo}}{b_0 \bullet (1-\beta)} \bullet L_{eff} \tag{11}$$

where L_{eff} is evaluated with the proposed equation (4).

Table 6 presents the analytically obtained results for the bending moment resistance considering the two analysed failure models: the Weynand proposal-based model (failure due to bending $M_{R,16F}$ and punching $M_{R,pun}$), and the Grotmann and Sedlaeck proposal-based model ($M_{R,FFR1}$). Additionally, the table includes the values of the experimental tests and the FE models. As shown in the table, the bending moment resistance of the front face of the tube ($M_{R,16F}$) is 30% lower than the failure associated with punching ($M_{R,pun}$). The moment-rotation experimental curves confirmed this fact. In most cases, the fixed indentation limit (3% of b_0) was reached before the failure of the specimen.

Finally, Figs. 19 and 20 show a graphical comparison of the moment resistance obtained experimentally and numerically (FEM model) against values obtained with both proposed models, $M_{R,16F}$ and M_{R_FFR1}. In both figures, the diagonal of the graph signifies the location where the experimental and simulated values coincide, and the dashed lines represent the locus of the points with an error between ±10 %. Both figures show that the second analytical proposal (FFR1) fits better than the first. In both cases, the average error when compared to the experimental results and the FEM results is 14 % and 15 %, respectively.

4.3. Characterisation of the lateral face component (LFC)

The expression proposed to calculate the stiffness of the lateral face is a modification of the equation in section 6.3.2 of Eurocode 3.1.8 [10], which refers to the shear stiffness of the web of an open cross-section. In rectangular hollow sections, the shear force is distributed over two web panels (lateral faces):

$$k_v = \frac{0.38 \bullet A_{VC}}{\beta_T \bullet z} \tag{12}$$

where k_v is the stiffness coefficient of the lateral face, A_{VC} is the shear area of the RHS, β_T is a transformation parameter according to Table 5.4 of Eurocode 3.1.8, and z is the lever arm.

The stiffness obtained using the proposed method and the experiments are compared in Table 7. The experimental data correspond to the results of experimental phase 5. The analytical stiffness was obtained by combining the stiffness of the lateral faces under tension and compression (k_{LF}) [20] and under shearing (k_v). The average error obtained is 8.1 %, signifying a close approximation of the proposed expression to the actual behaviour.

Regarding the resistance, the adapted expression was that outlined in section 6.2.6.1 of Eurocode 3.1.8. The final expression is:

$$F_v = \frac{0.90 \bullet f_{y,wc} \bullet A_{VC}}{\sqrt{3}} \tag{13}$$

where $f_{y,wc}$ and A_{vc} are the elastic limit and the shear area of the RHS, respectively.

Table 8 presents a comparison between the proposed method and the experimental results. The experimental maximum shear force in the lateral faces, by dismissing in a very conservative way the shear forces in the column over and under the joint, was calculated using the following expression [30]:

$$V_{max,exp.} = \frac{M_{R,exp}}{z} \tag{14}$$

As shown in Table 8, even with the above-mentioned conservative calculation, the experimental shear force in the lateral faces of

Table 5
Analytical stiffness for models $k_{FF,1}$ and $k_{FF,2}$

Specimen	β	k_{LF} [mm]	$k_{FF,1}$ [mm]	$S_{j,k_{FF1}}$ [kNm/rad]	$k_{FF,2}$ [mm]	$S_{j,k_{FF2}}$ [kNm/rad]
1.3*	0.74	2.65	2.64	2227	3.57	2561
1.4*	0.74	2.43	2.02	1828	2.87	2179
1.6	0.74	2.67	2.33	2035	3.11	2348
1.8	0.75	1.60	0.56	706	0.91	979
2.3*	0.73	2.44	2.49	2219	3.21	2497
2.4*	0.74	2.36	2.26	2060	3.03	2368
2.6	0.75	2.33	1.97	2011	2.88	2425
2.8	0.74	1.56	0.54	786	0.78	968
3.2	0.81	2.58	1.74	5318	2.14	5982
3.3	0.62	2.59	0.48	1111	0.58	1298
3.6	0.80	2.50	1.72	5694	1.94	6112
3.7	0.61	2.48	0.46	1211	0.54	1378
3.10	0.79	2.51	1.93	6242	2.05	6460
3.11	0.61	2.51	0.53	1335	0.63	1540
3.13	0.78	3.34	4.55	8691	4.00	8215
3.14	0.60	3.34	1.24	2280	1.37	2443
4.7*	0.82	1.59	1.44	1722	1.59	1814
4.8*	0.82	1.60	1.46	1729	1.60	1815
4.10*	0.83	1.55	1.48	1661	1.72	1789
4.11*	0.84	1.55	1.48	1656	1.99	1902
4.13*	0.75	1.54	0.55	722	0.84	966
4.14*	0.74	1.54	0.55	713	0.79	927

Table 6
Analytical, computational (FEM) and experimental moment resistance for specimens tested.

Specimen	β	$M_{R,pun}$ [kNm]	$M_{R,16F}$ [kNm]	$M_{R,FFR1}$ [kNm]	$M_{R,FEM}$ [kNm]	$M_{R,exp}$ [kNm]
1.3*	0.74	23.7	17.0	22.0	19.0	17.8
1.4*	0.74	19.9	14.1	18.7	19.2	17.2
1.6	0.74	22.6	16.1	20.9	20.1	18.5
1.8	0.75	9.5	6.4	8.3	9.6	7.5
2.3*	0.73	22.6	16.2	21.1	18.4	17.0
2.4*	0.74	21.8	15.2	20.1	21.2	15.4
2.6	0.75	17.2	12.0	15.8	18.5	17.6
2.8	0.74	8.2	5.3	6.9	10.1	9.6
3.2	0.81	40.4	29.2	39.0	45.5	43.1
3.3	0.62	24.6	14.5	19.1	19.0	19.6
3.6	0.80	33.6	24.0	31.8	39.8	37.9
3.7	0.61	20.3	11.9	15.7	17.3	16.8
3.10	0.79	39.9	28.4	38.0	50.0	46.8
3.11	0.61	24.3	14.3	19.0	20.3	22.7
3.13	0.78	63.1	46.3	61.1	71.2	69.4
3.14	0.60	39.1	23.9	32.0	31.9	33.3
4.7*	0.82	10.1	7.2	10.1	11.9	12.7
4.8*	0.82	10.1	7.3	10.1	12.7	12.5
4.10*	0.83	9.9	7.1	9.8	12.3	11.2
4.11*	0.84	9.9	7.2	10.2	12.3	11.6
4.13*	0.75	7.9	5.3	7.0	8.6	8.9
4.14*	0.74	7.9	5.2	6.8	8.5	8.6

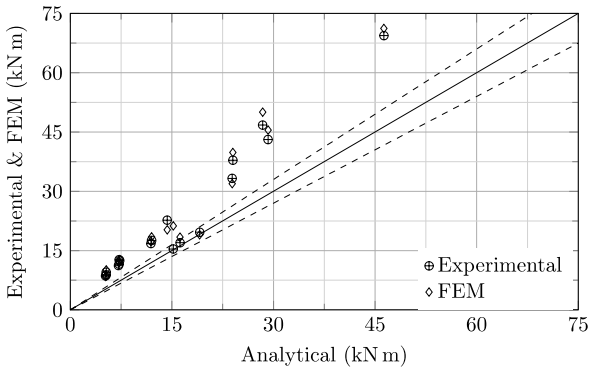

Fig. 19. Comparison of analytical moment resistance $M_{R,16F}$ vs experimental and FEM values.

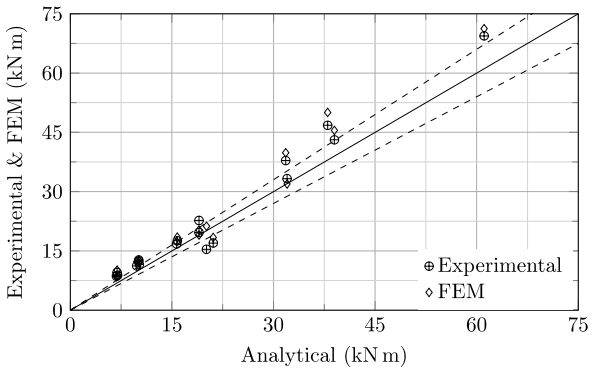

Fig. 20. Comparison of analytical moment resistance $M_{R,FFR1}$ vs experimental and FEM values.

the column is well under the supposed resistance, and the difference is above 200 %. This demonstrates that, in these cases, the behaviour of the lateral faces under shear was not limiting the strength of the joint, and further research on joints having this failure mode would be necessary to provide an accurate estimation.

Table 7
Analytical and experimental stiffness of one-sided beam joint.

Specimen	RHS	IPE	k_v [mm]	k_{LF} [mm]	$S_{ini.ana.}$ [kNm/rad]	$S_{ini.exp.}$ [kNm/rad]	Error [%]
5 1	200 × 150 × 6	300	2.97	2.42	15110	16415	7.9%
5 2	200 × 150 × 8	300	3.84	3.37	20583	22411	8.2%

Table 8
Analytical and experimental shear resistance of one-sided beam joint.

Specimen	RHS	IPE	F_v [kN]	$V_{max.exp.}$ [kN]	Diff. [%]
5 1	200 × 150 × 6	300	787.31	257.6	205.6%
5 2	200 × 150 × 8	300	1194.16	335.8	255.7%

5. Conclusions

This research aimed to investigate two novel welded I-beam–RHS-column joint components. To achieve this aim, both an experimental and computational programme were implemented. As a result of these campaigns, new expressions are proposed for use in the component method. The following are the primary conclusions drawn:

- Ten joints with less than one column-beam width ratio (β) were tested to characterise the tube front face component (FFC) under tension and compression. Additionally, two joints with asymmetrical loads were examined to understand the behaviour of the lateral face component (LFC) under shearing.
- A notable disparity in active components for joints with a beta value inferior to one was identified. Large indentations were observed in the interaction region between the tubular wall and the compressed IPE flange, along with tearing in the tension zone during large deformations.
- High stress concentrations were observed in asymmetrical load experiments at the contact zone between the tube and beam flanges. The lateral faces of the tube behaviour are dominated by the thickness of the wall tube, as depicted in the figures.
- Experimental findings reveal that width ratio (β) and column thickness (t_0) significantly affect joint stiffness, demonstrating that typical joints tend toward semi-rigidity and can achieve nominal rigidity by increasing β, as indicated by Eurocode stiffness classifications.
- Post-experimental programme, finite element models were developed and calibrated to replicate results. The outcomes demonstrated a high degree of concordance with the experiments, both for the initial rotational stiffness (average error: 13.8%) and for the moment resistance (average error: 8.4%).
- Analytical expressions are proposed for the front face (FFC) and lateral face component (LFC) based on experimental and FEM data.
- The models k_{FF2} and $M_{R,FFR1}$ provided the most accurate approximations of the FF component, with average errors of 11% and 15% respectively.
- Eurocode equation accurately characterized LFC stiffness (average error: 11%). However, the adapted Eurocode equation for resistance could not be tested as a failure source. Therefore, further research is needed to understand the behaviour of the lateral faces and its impact on joint strength.

CRediT authorship contribution statement

Javier Gracia: Data curation, Validation, Visualization, Writing – original draft, Writing – review & editing. **Miguel Lozano:** Data curation, Formal analysis, Investigation, Visualization, Writing – review & editing. **Carlos López-Colina:** Formal analysis, Investigation, Project administration, Supervision, Validation, Writing – original draft, Writing – review & editing. **Miguel A. Serrano-López:** Conceptualization, Funding acquisition, Investigation, Methodology, Supervision, Writing – review & editing.

Declaration of competing interest

The authors declare that they have no known competing financial interests or personal relationships that could have appeared to influence the work reported in this paper.

Data availability

Data will be made available on request.

Acknowledgements

The Spanish R&D National Program supported this research as a part of project BIA2013-43177-P, and it was also supported,

reviewed, and approved by the Committee for International Development and Education on Construction of Tubular Structures (CIDECT), as part of project 5CE.

The financial support by "ERDF A way of making Europe" through the grant PID2020-113895 GB-C33 funded by MCIN/AEI/10.13039/501100011033 are gratefully acknowledged.

References

[1] M. Eekhout, Tubular Structures in Architecture, CIDECT, Geneva, 2011.
[2] J. Wardenier, J.A. Packer, X.L. Zhao, G.J. van der Vegte, Hollow Sections in Structural Applications, second ed., CIDECT, Geneva, 2010.
[3] A.Y. Elghazouli, C. Málaga-Chuquitaype, J.M. Castro, A.H. Orton, Experimental monotonic and cyclic behaviour of blind-bolted angle connections, Eng. Struct. 31 (2009) 2540–2553, https://doi.org/10.1016/j.engstruct.2009.05.021.
[4] C. Málaga-Chuquitaype, A.Y. Elghazouli, Behaviour of combined channel/angle connections to tubular columns under monotonic and cyclic loading, Eng. Struct. 32 (2010) 1600–1616, https://doi.org/10.1016/J.ENGSTRUCT.2010.02.008.
[5] Y.C. Wang, L. Xue, Experimental study of moment–rotation characteristics of reverse channel connections to tubular columns, J. Constr. Steel Res. 85 (2013) 92–104, https://doi.org/10.1016/j.jcsr.2013.03.006.
[6] H.T. Thai, B. Uy, Rotational stiffness and moment resistance of bolted endplate joints with hollow or CFST columns, J. Constr. Steel Res. 126 (2016) 139–152, https://doi.org/10.1016/J.JCSR.2016.07.005.
[7] D. Gery, H. Long, P. Maropoulos, Effects of welding speed, energy input and heat source distribution on temperature variations in butt joint welding, J. Mater. Process. Technol. 167 (2005) 393–401, https://doi.org/10.1016/J.JMATPROTEC.2005.06.018.
[8] G.E. Linnert, Welding Metallurgy. Technology third ed., vol. 2, American Welding Society, Miami, 1997.
[9] J. Gracia, R. Goñi, E. Bayo, Stiffness metamodelling of 2D bolted extended end-plate steel connections using modal decomposition, J. Build. Eng. 34 (2021) 101925, https://doi.org/10.1016/j.jobe.2020.101925.
[10] CEN. Eurocode 3, Design of Steel Structures. Part 1-8: Design of Joints, 2005.
[11] Y. Kurobane, J.A. Packer, J. Wardenier, N. Yeomans, Design Guide 9 for Structural Hollow Section Column Connections, TÜV-Verlag GmbH, Cologne, 2005.
[12] L.H. Lu, The Static Strength of Uniplanar and Multiplanar Connections in Rectangular Hollow Sections, Delft University of Technology, 1997.
[13] T. Pitrakkos, W. Tizani, A component method model for blind-bolts with headed anchors in tension, Steel Compos. Struct. 18 (2015) 1305–1330, https://doi.org/10.12989/scs.2015.18.5.1305.
[14] S.H. Leong, N.H.R. Sulong, M. Jameel, Bolted connections to tubular columns at ambient and elevated temperatures - a review, Steel Compos. Struct. 21 (2016) 303–321, https://doi.org/10.12989/scs.2016.21.2.303.
[15] Y. Qin, Z. Chen, B. Rong, Component-based mechanical models for concrete-filled RHS connections with diaphragms under bending moment, Adv. Struct. Eng. 18 (2015) 1241–1255, https://doi.org/10.1260/1369-4332.18.8.1241.
[16] S. Di Benedetto, M. Latour, G. Rizzano, Chord failure resistance of 3D cut welded connections with CHS columns and through I-BEAMS, Thin-Walled Struct. 154 (2020) 106821, https://doi.org/10.1016/j.tws.2020.106821.
[17] A.Y. Park, Y.C. Wang, Development of component stiffness equations for bolted connections to RHS columns, J. Constr. Steel Res. 70 (2012) 137–152, https://doi.org/10.1016/j.jcsr.2011.08.004.
[18] K. Weynand, J.P. Jaspart, J.F. Demonceau, L. Zhang, Component Method for Tubular Joints | Draft Final Report No. 16F-3/15, Liège, 2015.
[19] J.P. Jaspart, K. Weynand, Design of hollow section joints using the component method, in: E. de M. Batista, P. Vellasco, L. Rodrigues (Eds.), Proceedings of 15th International Symposium on Tubular Structures, CRC Press, Rio de Janeiro, 2015.
[20] C. López-Colina, M.A. Serrano, M. Lozano, F.L. Gayarre, J.M. Suárez, T. Wilkinson, Characterization of the main component of equal width welded I-beam-to-RHS-column connections, Steel Compos. Struct. 32 (2019) 337–346, https://doi.org/10.12989/scs.2019.32.3.337.
[21] HTG de Barros, MM de Oliveira, A.M.C. Sarmanho, V.N. Alves, Stiffness assessment of welded I-beam to RHS column connections, Eng. Struct. 267 (2022) 114661, https://doi.org/10.1016/j.engstruct.2022.114661.
[22] M.A. Serrano-López, C. López-Colina, Y.C. Wang, M. Lozano, F.L. Gayarre, Comparative behaviour of 'I beam- RHS column' joints with and without web weld, J. Constr. Steel Res. 159 (2019) 330–340, https://doi.org/10.1016/j.jcsr.2019.05.002.
[23] L.H. Lu, G.D. de Winkel, Y. Yu, J. Wardenier, Deformation limit for the ultimate strength of hollow section joints, in: P. Grundy, A. Holgate, B. Wong (Eds.), Proceedings of the Sixth International Symposium on Tubular Structures, 1994. Melbourne.
[24] ANSYS, ANSYS 17.0 Release Notes, 2016.
[25] M.A. Serrano-López, C. López-Colina, J. González, F. López-Gayarre, A simplified FE simulation of welded I beam-to-RHS column joints, International Journal of Steel Structures 16 (2016) 1095–1105, https://doi.org/10.1007/s13296-016-0028-5.
[26] CEN. Eurocode 3, Design of Steel Structures. Part 1-5, Plated Structural Elements, 2006.
[27] CEN. Eurocode 3, Design of Steel Structures. Part 1-3: General Rules. Supplementary Rules for Cold-Formed Members and Sheeting, 2006.
[28] C. López-Colina, M. Serrano, M. Lozano, F. Gayarre, J. Suárez, Simplified models for the material characterization of cold-formed RHS, Materials 10 (2017) 1043, https://doi.org/10.3390/ma10091043.
[29] D. Grotmann, G. Sedlacek, Rotational Stiffness of Welded RHS Beam-To-Column Joints, Institute of Steel Construction, 1998. Final Report No. 5BB–8/98.
[30] J.-P. Jaspart, K. Weynand, Design of Joints in Steel and Composite Structures, Wilhelm Ernst & Sohn Verlag fur Architektur und technische Wissenschaften, Berlin, Germany, 2016.